





Field Tests on a Full-Scale Steel Chimney Subjected to Vortex-Induced Vibrations

Øyvind Mortveit Ellingsen , PhD student, CSTB, Nantes, France; LadHyx, CNRS-Ecole polytechnique, IP-Paris, France; Olivier Flamand , Engineer, CSTB, Nantes, France; Xavier Amandolese , Assoc. Prof., Dr, PhD, LadHyx, CNRS-Ecole polytechnique, IP-Paris, France; LMSSC, CNAM, Paris, France; Francois Coiffet, PhD, Dr, CERIC, Poujoulat Group, Granzay-Gript, France; Pascal Hémon , PhD, Dr, LadHyx, CNRS-Ecole polytechnique, IP-Paris, France.

Contact oyvind-mortveit.ellingsen@polytechnique.edu

DOI: 10.1080/10168664.2021.1936352

Abstract

Industrial chimneys, launch vehicles and stacks are examples of large diameter circular cross section structures that can be prone to cross-wind vortex-induced vibration (VIV). VIV has been extensively studied for both fundamental and applied issues, but few documented studies concern high Reynolds number regimes ($>5 \times 10^5$) in atmospheric turbulent wind. This paper introduces a field test on a slender light and low damped chimney designed to experience “super-critical” VIV at moderate wind velocity. The chimney was recently erected in a wind monitored field, near the Atlantic coast of France. The purpose of this paper is to present the first vibration results obtained during a sequential 13-day period in September 2020. A statistical analysis has been performed on the amplitude and dominant frequency responses and results are reported in term of probability distribution as a function of wind speed and direction. VIV events of low ($<15\%$ of diameter) to moderate amplitude ($>30\%$ of diameter) have been highlighted in a range of wind velocity 25% lower than expected, along with significant influence of the wind direction – low turbulence easterly wind giving vortex-induced vibrations with the highest amplitude.

Keywords: : Vortex-induced vibration; super-critical Reynolds number; full-scale experiment; chimney; atmospheric boundary layer; turbulence intensity

Introduction

Slender structures of circular cross section can be prone to vibrations under wind effects and must be designed and/or treated accordingly. For an isolated tower, stack or chimney, two kinds of vibrations are generally considered: in-line vibrations due to atmospheric turbulence and cross-wind vibrations due to the vortex signature. The former concerns extreme wind speed and is the consequence of random aerodynamic load due to turbulence. Since this load can be considered as independent of the structure’s dynamic response, the problem can be addressed using well-accepted random vibration methods or simplified equivalent static formulations (see for example Refs. [1,2]). The latter is more complex. It is the consequence of a nonlinear coupling between the fluid force due to the Karman vortex wake and the chimney’s motion. This phenomenon, known as vortex-induced vibration (VIV), has been extensively studied

for both fundamental and applied issues (see for example Refs. [2–4] for a review).

VIV is characterized by significant oscillations of self-limited amplitude in a limited velocity range where the wake frequency is controlled by the motion, a phenomenon referred to as “lock-in”. Both the oscillation amplitude and the range of lock-in strongly depend on the structure-to-fluid mass ratio and on the damping ratio of the structure. This is encapsulated in the Scruton number (Sc , a dimensionless mass-damping ratio parameter) with low values leading to higher vibration amplitudes and a wider lock-in range. The Reynolds number and turbulence characteristic of the incoming flow can also have significant impact on the VIV of a slender structure in an atmospheric boundary layer.^{5,6} It is well established that the VIV response is strong for low turbulence flow in the sub-critical Reynolds number regime ($<3 \times 10^5$) but comparatively negligible in the critical-transitional

Reynolds number regime, and that a recovering VIV response can be observed in the super-critical Reynolds number regime ($>10^6$).⁵

Tall industrial chimneys, launch vehicles and stacks are examples of large diameter circular cross section structures that can be prone to vortex-induced vibrations at super-critical Reynolds numbers in atmospheric turbulent wind. It is then necessary to validate an appropriate methodology for their design and/or the design of additional damping devices (cf. Ref. [7] for simulations on the effect of additional damping devices). VIV models are numerous, and codified methods can be found in many standards, but their ability to capture the VIV amplitude response at super-critical Reynolds numbers and with real atmospheric boundary layers needs validation. Wind tunnels are also important in response prediction, although scaled models can cause cross-wind loads to be highly overestimated.⁸ A method for overcoming the scaling effect is to increase the Reynolds number artificially by adding surface roughness to the cylinder’s surface.^{4,9} While this can satisfactorily change the vortex wake signature (e.g. mean drag and r.m.s. lift) for a fixed cylinder, the impact on a 3D slender cylinder during lock-in is less clear, and wind tunnel studies have led to various conclusions, so it needs to be investigated further.^{10–13}

Continuous measurements from monitored industrial chimneys can be found in the literature,^{14–20} but the monitoring was often limited to acceleration data and a reference velocity. These chimneys have been designed or treated to limit VIV, meaning that the observed vibrations were small. Additionally, the access and opportunity to install extra sensors were limited as they were in use. More response data on industrial chimneys

are available, but often only the maximum amplitudes are mentioned and are used to validate VIV models in design standards.^{21,22}

For other more well-studied circular structures using field experiments, there is a problem of dimensions.^{23,24,25} Owing to their smaller size, the high amplitude VIV response was at sub-critical or critical Reynolds numbers rather than super-critical. The same problem was observed in wind tunnels when using larger scale wind tunnel experiments,²⁶ as the speed needed to reach super-critical wind speed is large.

In that context, a custom-made 35.5 m steel chimney has been recently erected and instrumented in a monitored wind field in Bouin (near the Atlantic coast of France). This chimney was designed to have a low Scruton number ($Sc < 2$) and to experience “super-critical” VIV at moderate wind speeds (< 10 m/s). The paper is organized as follows: field test information and methodology including the structural characteristics of the chimney are presented in Section 3. Characterization of the incoming wind is reported in Section 4. Vibration results obtained during a sequential 13-day period in September 2020 are presented in Section 5, before the conclusions and outlook regarding this new test platform.

Field-test Platform Details and Methodology

Structural Characteristics of the Chimney

The chimney was designed, manufactured and erected by Beirens (Poujoulat group) during the summer of 2020. *Figure 1* shows a view of the chimney in the field. This custom-made steel chimney of height $h = 35.5$ m has a diameter $d_{\text{lower}} = 1$ m for its 12 m long bottom part and a diameter $d_{\text{top}} = 2$ m for its 20.5 m long upper part, with a 3 m long tapered connecting element (see *Fig. 2*). This unusual shape (for a chimney) was chosen to ensure vortex-induced vibrations in the super-critical Reynolds number range ($> 10^6$) at moderate wind speed (< 10 m/s) for the purpose of this experiment.

Structural characteristics of the chimney are given *Table 1*, along with the expected Reynolds number at the critical wind speed, referred to as Re_{VIV} .

The equivalent mass, m_e , has been calculated using Equation (1), where $\psi(z)$ is the shape of the first bending mode and $m(z)$ is the mass per unit height (both being identified during the design phase of the chimney using computer-aided design). Experimental tests performed at the beginning of the test series identified the first natural frequency, f_1 , as 0.78 Hz and allowed the identification of the associated damping ratio, ζ_1 . The Scruton number, calculated using formula (2), was rather low ($Sc = 1.82$) and a high amplitude response was expected. Using Eurocode’s recommendations,²⁷ the critical wind speed ($f_s = f_n$ with Strouhal number $St = 0.18$) was close to 8.7 m/s ($Re_{\text{VIV}} \approx 1.16 \times 10^6$) and the maximum dimensionless amplitude (normalized by the top diameter) would be either 0.31 (method 1 of Ruscheweyh⁵) or 0.53 (method 2 of Vickery and Basu⁶).

$$m_e = \frac{\int_0^h \psi(z)^2 m(z) dz}{\int_0^h \psi(z)^2 dz} \quad (1)$$

$$Sc = \frac{4\pi\zeta m_e}{\rho d^2} \quad (2)$$

It is important to note that, owing to a damaged bolt, the natural frequency decreased to around 0.71 Hz at the end of the experimental procedure. In that context, an increase in the associated damping ratio, which was not measured, is also suspected. This will be discussed further in Section 5.

Field-Test Location and Instrumentation

The chimney was mounted in a monitored wind field in Bouin (GPS coordinates 46,975, -1998), near the Atlantic coast of France. According to the Eurocode,²⁷ this area is in a wind zone category with a 50-year reference wind equal to 26 m/s. The site is surrounded by farmland with a sparse gathering of trees and the terrain category is classified as type II.²⁷ Owing to the remote location of the field, and the lack of nearby structures, the model chimney was designed without



*Fig. 1: Experimental chimney in the monitored field (the mast with wind anemometers is slightly visible, see *Fig. 2* for details)*

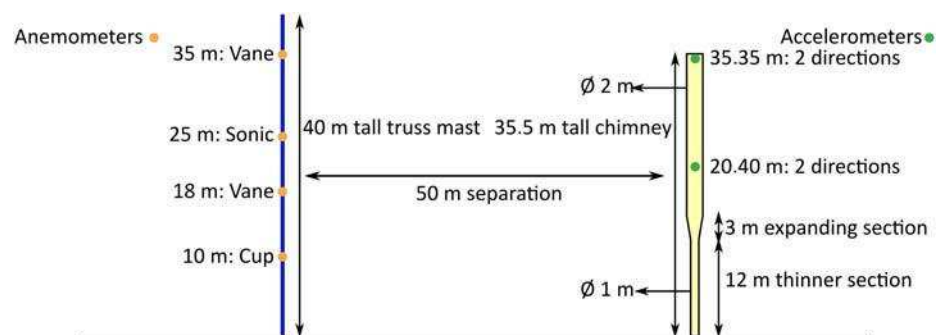


Fig. 2: Sketch of the chimney and anemometer’s mast, dimensions and locations of anemometers and accelerometer sensors

d_{top} (m)	d_{lower} (m)	h (m)	$h_{d=2m}$ (m)	m_e (kg/ m)	f_1 (Hz)	ζ_1 (%)	Sc (-)	Re_{VIV} (-)
2	1	35.5	20.5	322.6	0.78	0.22	1.82	1.16×10^6

Table 1: Structural characteristic of the chimney (as identified at the start of the experiment)

fear of loss of human life, animal life or damage to nearby structures.

The chimney was instrumented with two bi-directional accelerometers, one at 20.4 m and one at 35.35 m (near the top) as shown in Fig. 2. Their measuring range was ± 2 g and the acquisition frequency was set to 10 Hz. Wind velocity was measured at several heights using wind anemometers mounted to a 40 m tall truss mast, located 50 m northwest of the chimney (see Fig. 2). Vane anemometers, measuring speed and direction, were placed at heights of 18 and 35 m and a cup anemometer was located at 10 m. Both vane and cup anemometers record the wind statistics (mean, standard deviation, maximum speed and direction for the vane anemometers) over a 10-minute period. An additional sonic anemometer was located at 25 m height. It could measure the unsteady velocity (three components) at a rate of 5 Hz. While the recording frequency of the sonic anemometer was different from the accelerometers, the recordings were time-synchronized. The locations of the sensors are sketched in Fig. 2.

Data Analysis Process

Vibration and wind results shown in the present study are based on 1872 ten-minute records gathered at 35 m over a sequential 13-day period in September 2020. Additional wind data, gathered with all the anemometers distributed along the truss mast, were used to plot the mean and turbulent velocity profiles of the incoming wind.

Each sample of ten-minute top wind was analysed by first finding the mean velocity and dominant wind direction. As the accelerometer directions are constant, the displacements are transformed to cross and in-line vibrations using the direction of the incoming wind. This was used to calculate, using the top bi-directional accelerometer, an associated 10-minute cross-wind acceleration signal. The displacement, $y(t)$, was calculated from the acceleration signal using the inverse Fourier transform of the spectrum $Y(\omega)$ obtained from the Fourier

transform of the acceleration $A(\omega)$ and relation (4). A fifth-order high-pass Butterworth filter with cutoff frequency 0.3 Hz has been applied to the acceleration data to eliminate low frequency noise amplified by the Fourier identity²⁸

$$A(\omega) = -\omega^2 Y(\omega) \quad (4)$$

The Hilbert transform²⁹ was used to calculate the response envelopes of the displacement in order to obtain the mean, maximum and standard deviation of the displacement amplitude over a 10-minute recording. The associated dominant vibration frequency was identified by peak detection on the spectrum $Y(\omega)$.

For each ten-minute sample, two cross-wind vibration values were gathered: the maximum amplitude of vibration and the associated dominant frequency along with two wind values: the mean velocity and the dominant direction. Statistical analysis was performed using the 1872 samples in order to plot the probability distribution of the vibration amplitudes and associated dominant frequency as a function of wind velocity or

direction. These probability distributions were calculated using a statistical kernel function.³⁰ The kernel used here is the standard Gaussian kernel used in R and the ggplot2 library (versions 4.0.2 and 3.3.2, respectively).

Wind Characterization

Wind Speed and Directional Distribution

The top vane anemometer was used to create the “wind rose” plotted in Fig. 3, which shows the distribution of wind speeds and directions. The two most frequent wind directions were northwesterly and northeasterly. Additionally, the most frequently observed speed range was 4–6 m/s, with speeds above 6 m/s having a long tail and short tail for speeds below 4 m/s. When ignoring the direction, the distribution of all wind speeds resembles a discrete log-normal probability distribution or a negative binomial distribution. The probabilities of specific wind directions were found using their relative frequencies and are: S –4.4%, SW –1.5%; W –1.9%; NW –29.5%; N –16.8%; NE –31.4%; E –11.4% and SE –3.1%.

Using the measured wind speeds and $U_{crit} = 8.7$ m/s, the probability of seeing a speed above $0.8 U_{crit}$ (Eurocode’s recommendations for the onset of VIV), is 21.3%. As vortex-induced vibrations are only observed in a

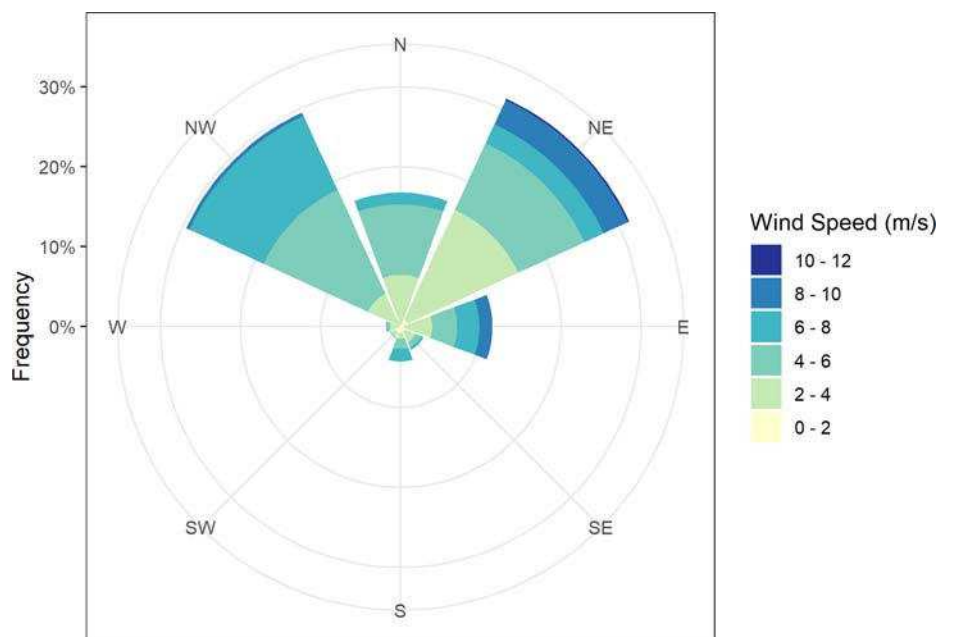


Fig. 3: Frequency of incoming wind velocity (with 8 directional bins) using the 10-minute mean directions and speeds at 35 m

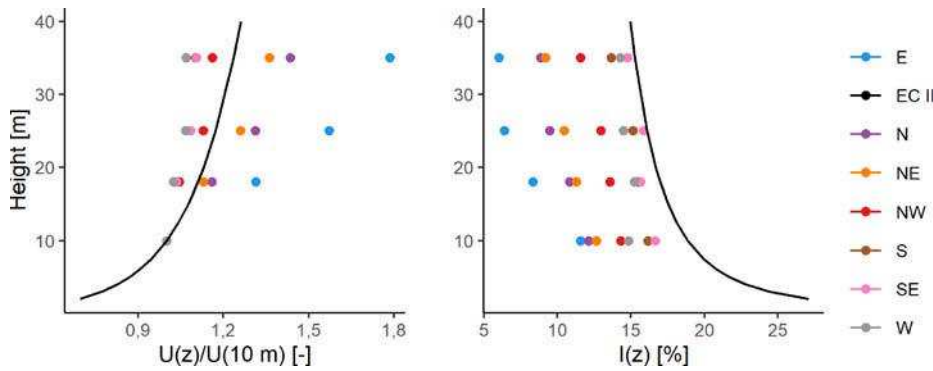


Fig. 4: Mean incoming speed and turbulence profiles (filled dots) compared with the Eurocode profile for terrain category II (solid lines)

specific speed range, an upper limit to the investigated wind speed range can be added and is defined as $1.2 U_{crit}$, which is when one of the Eurocode design methods gives the highest amplitude.²⁷ With this, 21.3% of the observed incoming wind speeds can be found in the vortex-induced wind speed range of 7–10.5 m/s. The two given percentages are the same, because 10.44 m/s was the maximum observed mean wind speed.

Wind Speed and Turbulence Profiles

The mean wind velocity and turbulence intensity evolution with height for all eight cardinal and ordinal directions are plotted in Fig. 4, gathering wind data over the anemometer masts for wind speeds greater than 5 m/s at 35 m height. The turbulence intensity $I(z)$, is defined as the standard deviation of speed at a given height divided by the corresponding mean speed. Eurocode mean wind velocity and turbulence profiles, for terrain category II are also plotted in Fig. 4.

It is evident that those mean velocity and turbulence profiles for which the ten-minute wind speed at 35 m remains lower than 12 m/s strongly depend on the wind direction. While the Eurocode type II mean velocity profile was close to a median profile in comparison with the experiments, the Eurocode type II turbulence profile overestimates the turbulence intensity for all directions. A direct comparison with Eurocode profiles, which concern reference wind (ten minutes at 10 metres) of higher mean value (50-year wind), should then be considered with some caution. Nevertheless, for this low-to-moderate wind speed investigation, some relevant

information regarding the incoming wind can be highlighted that will be useful for the vibration analysis.

The northwesterly wind, which has the highest probability of occurrence, has a mean velocity profile close to the Eurocode type II model but a turbulence intensity value lower by a half, with a value slightly less than 10% at 35 m. The easterly wind, which applies to 11.4% of the observed directions but highlights significant sequences of vortex-induced vibrations of the chimney, was characterized by an important speed gradient with height and a low turbulence intensity of less than 6% at 35 m. This means that wind coming from inland and headed towards the ocean has the strongest shear but the lowest mean turbulence intensity at the heights measured.

Cross-wind Vibrations of the Chimney

Following the data analysis process recalled in Section 3.3, a statistical analysis of the chimney's cross-wind vibration was performed. An example of build-up to vortex-induced vibrations and its steadiness during lock-in are shown in Fig. 5. This figure shows the displacement and amplitude envelope for a segment with easterly wind that starts at 4.5 m/s but steadily increased to above 5 m/s according to the sonic data. Statistical distributions of the maximum dimensionless amplitude of vibration (normalized with the top diameter) and associated dominant frequency (normalized with the chimney's natural frequency) are plotted in Figs 6, 7 as a function of wind velocity.

Results are reported using violin plots, mirroring the probability distribution of the data along the y-axis as a function of discrete wind speed groups (nominal speed value ± 0.25 m/s). The exceptions are for 1.25 and 10.25 m/s, which groups all speeds below 1.5 and above 10 m/s, respectively. In addition to the violin plot, boxplots highlighting the summary statistics (median and quartiles) are shown. One benefit of violin plots over boxplots is that they show the distribution of the data. This is particularly relevant for multimodal processes³⁰ for which the most likely value, associated to

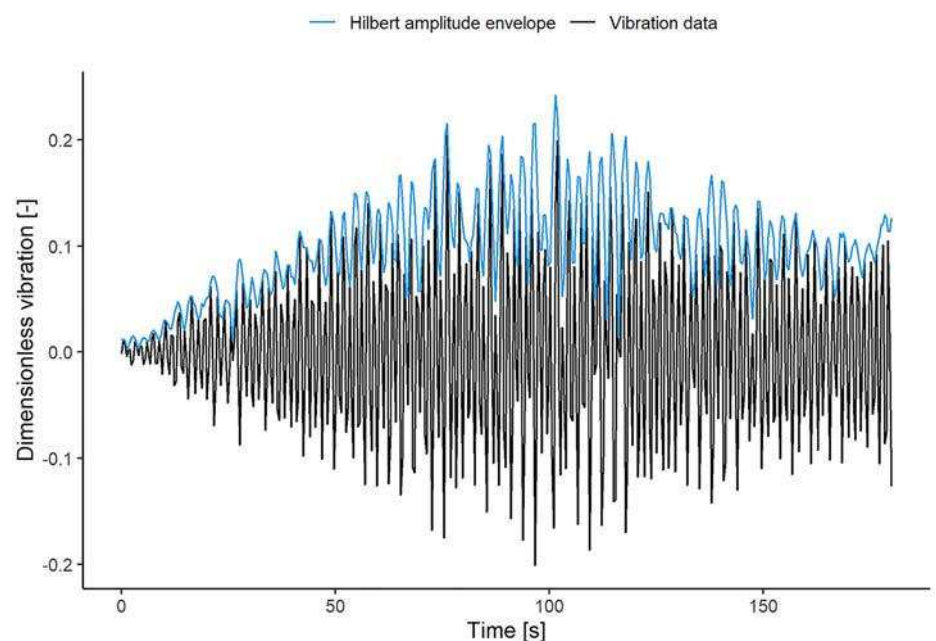


Fig. 5: Example of cross-wind displacement signal with build-up to vortex-induced vibrations and the vibration during lock-in at 5 m/s

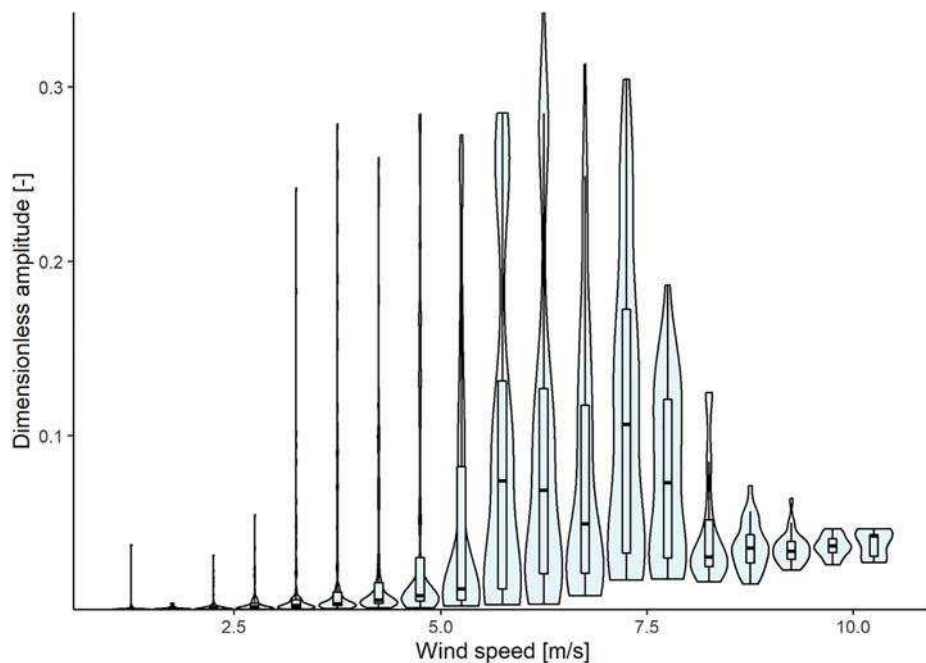


Fig. 6: Probability distributions of maximum dimensionless amplitude (normalized with tip diameter) at given speed range. The interior rectangle and lines are boxplots showing summary statistics

the widest point of the violin shape, can differ from the median value. It should also be noted that, for the sake of visibility, the mirrored probability distributions shown in Figs. 6–8 were scaled so that their widths were fixed for all speeds. Moreover, the tails of the probability distributions, which contain artifacts of the kernels used, were removed from these plots.

As pointed out in Section 4.2, the direction of the incoming wind strongly affects the mean wind velocity and turbulence intensity profiles. So significant impact of the wind direction on the chimney's cross-vibration would then be expected. Statistical distributions of the maximum dimensionless amplitude of vibration are then plotted in Fig. 8 as a function of wind direction. The direction groups used

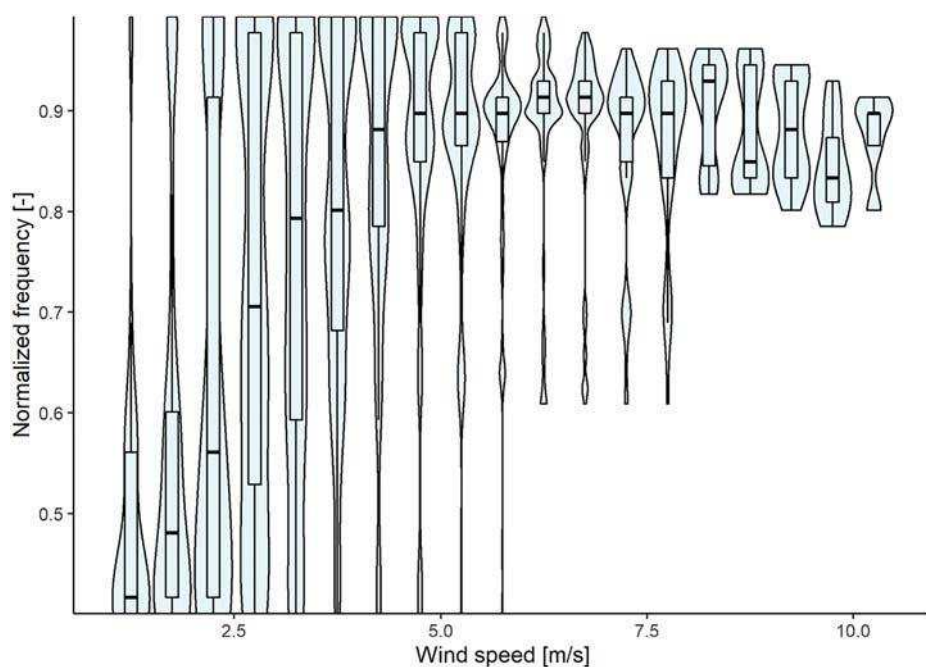


Fig. 7: Probability distributions of the dominant frequency of motion (normalized with chimney's first natural frequency) at given speed range. The interior rectangle and lines are boxplots showing summary statistics

in Fig. 8 were the cardinal and ordinal directions $\pm 22.5^\circ$, with $0 \pm 22.5^\circ$ defined as northerly wind and $90 \pm 22.5^\circ$ as easterly. Both of the groups were based on the mean values from the vane anemometer at 35 m.

Figure 6 clearly shows that cross-wind vibrations of significant amplitude can be observed for wind speeds between 5 and 8.5 m/s with a maximum amplitude up to 35% of the diameter (0.7 m) observed at speeds between 6 and 6.5 m/s. This maximum amplitude was close to the one calculated using Eurocode's method 1 (based on Ruscheweyh's approach⁵) and 35% lower than the one calculated using Eurocode's method 2 (based on Vickery and Basu's approach⁶). However, this maximum amplitude was observed at a wind speed 2 m/s lower than the one recommended by Eurocode, suggesting a higher Strouhal number value (closer to 0.25) at high Reynolds number ($Re \approx 8.3 \times 10^5$ for $U = 6.25$ m/s).

At speeds below 5 m/s, there were cases of amplitudes greater than 20% of the diameter. In most of these cases, the mean speed was slowly reducing from the VIV lock-in speed region over several 10-minute recordings. The vibration amplitude continued to be high and it was possible for high amplitude VIV to continue until mean wind speeds as low as 3.3 m/s. In a few other cases, high amplitude responses could be due to the speed increasing towards the end of the 10-minute recording.

Lower amplitude levels (less than 15% of diameter) were also observed in the wind speed range 5–8.5 m/s. Based on the shape of the violin plot, the lower amplitude vibrations have higher conditional probability than the high amplitude vibrations. The statistical distributions of the maximum amplitude as a function of the wind direction, reported in Fig. 8, suggest that the lower VIV data are likely to be attributable to northwesterly wind, which was the most frequently observed direction, and that the sequences of vortex-induced vibrations with the highest amplitude were due to the low turbulence easterly wind.

No vibration amplitudes greater than 7.5% of the diameter were observed for wind speeds higher than 8.5 m/s. From 8.5 to 10.25 m/s (which groups

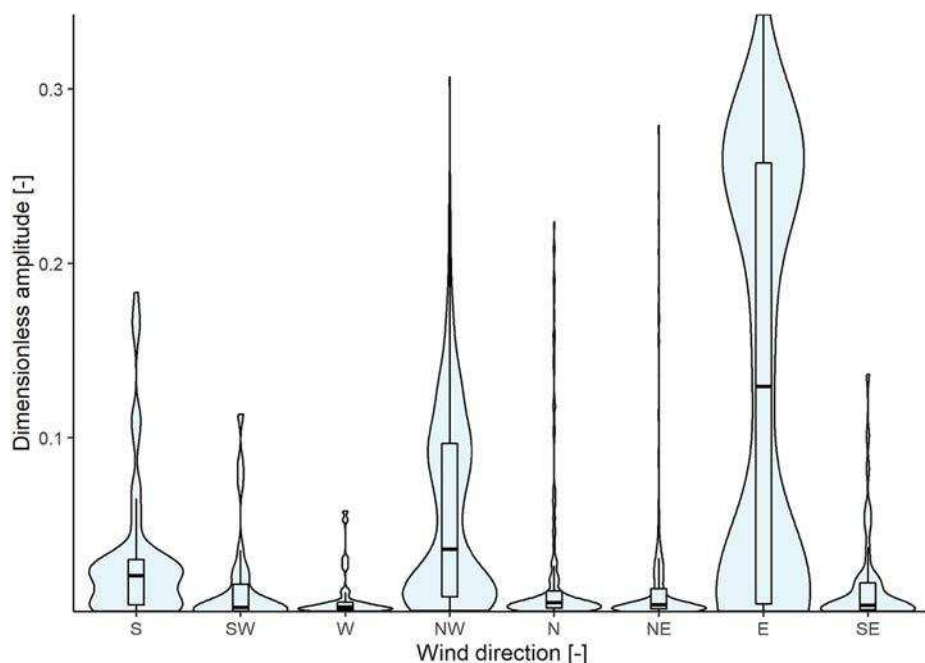


Fig. 8: Probability distributions of maximum dimensionless amplitude (normalized with tip diameter) for different directions $\pm 22.5^\circ$. The interior rectangle and lines are boxplots showing summary statistics

all speeds above 10 m/s), one can observe that the probability distributions of the maximum amplitude are more centred with a median value gradually increasing with the velocity. The vibrations can then be due to turbulence-induced vibrations. In this range of wind velocities, the probability distributions of dominant frequency are more surprising. For turbulence-induced vibrations one would expect a dominant frequency close to the first natural frequency of the chimney (and thus a dominant normalized frequency close to one). Nevertheless, the shape of the violin plot reveals two areas of high probability for the dominant frequency (see for example Fig. 7, for $U = 8.75$ m/s), one with normalized frequencies between 0.9 and 1 and the other with normalized frequencies between 0.8 and 0.9. As reported in Section 3.1, a damaged bolt was observed at the end of the test series. A check showed a decrease of 10% for the chimney's first natural frequency that could explain this peculiar distribution of the dominant frequency in this turbulence-induced vibration regime.

Even if the probability of occurrence of cross-vibrations with significant amplitude was rather low below 5 m/s, it is interesting to focus on the evolution of the probability distribution of the dominant frequency

with wind speed before lock-in (see Fig. 7). Up to 4.75 ± 0.25 m/s, two distinct frequency groups can be highlighted. One group contains the median frequency, which increases almost linearly with wind speed, while the other group contains normalized frequencies between 0.9 and 1 with increasing conditional probability with speed. The first group is clearly related to the vortex shedding signature while the second is due to turbulence-induced vibrations.

Relevant information on the response can be found in Fig. 8, which shows the statistical distributions of maximum amplitude as a function of wind direction. Easterly (low turbulence) winds were the most favourable to generate high amplitude (>30% of the top diameter) vortex-induced vibrations. Easterly winds also have the highest conditional probability of maximum amplitudes greater than 15% of the diameter (near 50% of the maximum amplitudes were above 15% of the diameter). Vortex-induced vibrations were also observed with the more turbulent northwesterly winds, but with lower amplitudes of vibration. Vibrations up to 18% of the diameter were observed for southerly winds but with a low probability of occurrence. The shape of the violin plot for southerly directions shows a high conditional probability for vibrations lower than 5% of the top

diameter, and this could be due to turbulence induced vibration (according to Fig. 4, the turbulence intensity was high, close to 15% at 35 m height, for southerly winds). The conditional probability of wind speeds in the range 5–8 m/s was higher for easterly, northwesterly and southerly winds (it was 59.6% for northwesterly winds, 47.6% for southerly and 42.7% for easterly winds, see Fig. 3). For northerly and northeasterly winds, on the other hand, it's much more likely to see speeds below 5 m/s and the most likely amplitudes were low. This might be a reason why the first three mentioned directions have higher conditional probability for vortex-induced vibrations of significant amplitude. Easterly winds (towards the ocean) also had the strongest speed gradient with height and the lowest turbulence intensity (less than 6% at a height of 35 m in comparison with 12% for northwesterly winds). While the full impact of shear flow on vortex wake signature and VIV is not well understood, it is well known that VIV is stronger for low turbulent flow in 2D experiments.^{2,8,12,31,32} This is also shown in the present study in the presence of atmospheric boundary layers with different turbulence intensity profiles.

Conclusion

A custom-made chimney having large top diameter (2 m) and low Scruton number ($Sc = 1.82$) was erected in a monitored wind field near the Atlantic coast of France. Details of the field-test platform and methodology, including the structural characteristics of the chimney and the wind "potential", have been presented. Preliminary vibration results, obtained during a sequential 13-day period in September 2020, were presented and discussed. Amplitude and frequency responses were reported in term of probability distributions plotted as a function of both wind speed and direction. As expected, two types of cross-wind vibrations were observed, turbulence-induced vibrations and vortex-induced vibrations.

Vortex-induced vibrations of significant amplitude were mostly observed for wind speeds between 5 and 8.5 m/s with maximum amplitude near 6.25 m/s. This "critical" velocity value was lower than expected,

suggesting a higher Strouhal number (closer to 0.25) for high Reynolds numbers ($Re \approx 8.3 \times 10^5$ for $U = 6.25$ m/s). Several VIV events of low (<15% of the diameter) to moderate amplitude (>30% of the diameter) were observed with lower amplitudes being more likely. The results also show that easterly (low turbulence) winds were mainly responsible for the highest amplitudes of vibration (>30% of the top diameter) while the low amplitude VIV responses were mainly due to northwesterly and southerly winds having higher turbulence intensity.

The goal of this test platform was to gather VIV data at super-critical Reynolds numbers in real atmospheric winds. These preliminary results will help to forecast specific VIV events on this chimney in order to strengthen the present results and perform additional unsteady pressure measurements so as better to understand the 3D vortex signature, loading and VIV response at “super-critical” Reynolds numbers and for different turbulence conditions.

Acknowledgements

Special acknowledgement is extended to Aurélien Jeannoton (of Beirens) for designing and constructing the chimney used in the field experiment.

Funding

This work is part of a partnership co-funded by Beirens (of the Poujoulat Group), Centre Scientifique et Technique du Bâtiment (CSTB), Centre National d’Etudes Spatiales (CNES) and LadHyX, CNRS-Ecole polytechnique.

ORCID

Øyvind Mortveit Ellingsen  <http://orcid.org/0000-0001-7720-6670>

Olivier Flamand  <http://orcid.org/0000-0002-4885-1117>

Xavier Amandolese  <http://orcid.org/0000-0001-5346-9871>

Pascal Hémon  <http://orcid.org/0000-0002-7220-1392>

References

[1] Davenport AG. The spectrum of horizontal gustiness near the ground in high winds. *Q J R Meteorol Soc.* 1961 Apr;87(372):194–211.

[2] Simiu E, Scanlan RH. *Wind effects on structures: fundamentals and applications to design.* New York (NY): Wiley; 1996.

[3] Blevins RD. *Flow-induced vibration.* 2nd ed. Malabar, FL: Krieger Pub Co; 2001.

[4] Paidoussis MP, Price SJ, de Langre E. *Fluid-structure interactions cross-flow-induced instabilities.* Cambridge, New York: Cambridge University Press; 2010.

[5] Ruscheweyh H. Vortex excited vibrations. In: Sockel H, editor. *Wind-excited vibrations of structures.* Vienna: Springer; 1994. p. 51–84.

[6] Vickery BJ, Basu RI. Across-wind vibrations of structures of circular cross-section. Part I. Development of a mathematical model for two-dimensional conditions. *J Wind Eng Ind Aerod.* 1983; 12(1): 49–73.

[7] Blanchard A, Bergman LA, Vakakis AF. Vortex-induced vibration of a linearly sprung cylinder with an internal rotational nonlinear energy sink in turbulent flow. *Nonlinear Dyn.* 2020 Jan 1; 99(1): 593–609.

[8] Vickery BJ, Daly A. Wind tunnel modelling as a means of predicting the response of chimneys to vortex shedding. *Eng Struct.* 1984 Oct 1; 6(4): 363–368.

[9] Ribeiro JLD. Effects of surface roughness on the two-dimensional flow past circular cylinders I: mean forces and pressures. *J Wind Eng Ind Aerod.* 1991 Apr; 37(3): 299–309.

[10] Batham JP. Wind tunnel tests on scale models of a large power station chimney. *J Wind Eng Ind Aerod.* 1985; 18(1): 75–90.

[11] Cheng C, Kareem A. Acrosswind response of reinforced concrete chimneys. *J Wind Eng Ind Aerod.* 1992 Jan; 43(1–3): 2141–2152.

[12] Fox TA, West GS. Fluid-induced loading of cantilevered circular cylinders in a low-turbulence uniform flow. Part 2: fluctuating loads on a cantilever of aspect ratio 30. *J Fluids Struct.* 1993 Jan 1; 7(1): 15–28.

[13] Stansby PK. The locking-on of vortex shedding due to the cross-stream vibration of circular cylinders in uniform and shear flows. *J Fluid Mech.* 1976 Apr; 74(4): 641–665.

[14] Christensen O, Askegaard V. Wind forces on and excitation of a 130-m concrete chimney. *J Wind Eng Ind Aerod.* 1978; 3(1): 61–77.

[15] Hansen SO. Cross-wind vibrations of a 130-m tapered concrete chimney. *J Wind Eng Ind Aerod.* 1981 Jul; 8(1–2): 145–155.

[16] Hirsch G, Ruscheweyh H. Full-scale measurements on steel chimney stacks. *J Wind Eng Ind Aerod.* 1975 Jan; 1: 341–347.

[17] Melbourne WH, Cheung JCK, Goddard CR. Response to wind action of 265-m mount Isa stack. *J Struct Eng.* 1983; 109(11): 2561–2577.

[18] Müller FP, Nieser H. Measurements of wind-induced vibrations on a concrete

chimney. *J Wind Eng Ind Aerod.* 1975; 1: 239–248.

[19] Sanada S, Suzuki M, Matsumoto H. Full scale measurements of wind force acting on a 200 m concrete chimney, and the chimney’s response. *J Wind Eng Ind Aerod.* 1992 Jan; 43(1–3): 2165–2176.

[20] Waldeck JL. The measured and predicted response of a 300 m concrete chimney. *J Wind Eng Ind Aerod.* 1992 Oct; 41(1–3): 229–240.

[21] Lipecki T, Bec J, Jamińska P. A comparative study of along-wind and crosswind responses of steel chimneys according to Polish and Eurocode standards. *Czasopismo Techniczne;* 2016; 2-B(12): 107–126.

[22] Lupi F, Niemann H-J, Höffer R. A novel spectral method for cross-wind vibrations: application to 27 full-scale chimneys. *J Wind Eng Ind Aerod.* 2017; 171: 353–365.

[23] Galemann T, Ruscheweyh H. Measurements of wind induced vibrations of a full-scale steel chimney. *J Wind Eng Ind Aerod.* 1992 Oct; 41(1–3): 241–252.

[24] Zuo D. Full-scale measurement of wind pressure on the surface of an oscillating circular cylinders. *J Wind Eng Ind Aerod.* 2014 Oct; 133: 65–79.

[25] Ruscheweyh H, Galemann T. Full-scale measurements of wind-induced oscillations of chimneys. *J Wind Eng Ind Aerod.* 1996 Dec; 65(1–3): 55–62.

[26] Belloli M, Giappino S, Morganti S, Muggiasca S, Zasso A. Vortex induced vibrations at high Reynolds numbers on circular cylinders. *Ocean Eng.* 2015; 94: 140–154.

[27] Eurocode. 1: *Actions on structures, part 1–4: general actions (EN–1991).* Eurocode. 1: Actions on structures, Part 1 – 4: General Actions (EN–1991). Brussels: Eurocode; 2010.

[28] Meirovitch L. *Fundamentals of vibrations.* Long Grove (Illinois): Waveland Press, 2010.

[29] Cohen L. *Time-frequency analysis.* Englewood Cliffs (NJ): Prentice Hall PTR; 1995. 299 p. (Prentice Hall signal processing series).

[30] Wickham H. *ggplot2: elegant graphics for data analysis.* 2nd ed. New York, NY: Springer-Verlag; 2016. 1 p. (Use R!).

[31] Basu RI, Vickery BJ. Across-wind vibrations of structure of circular cross-section. Part II. Development of a mathematical model for full-scale application. *J Wind Eng Ind Aerod.* 1983; 12(1): 75–97.

[32] Ribeiro JLD. Effects of surface roughness on the two-dimensional flow past circular cylinders II: fluctuating forces and pressures. *J Wind Eng Ind Aerod.* 1991 Apr; 37(3): 311–326.